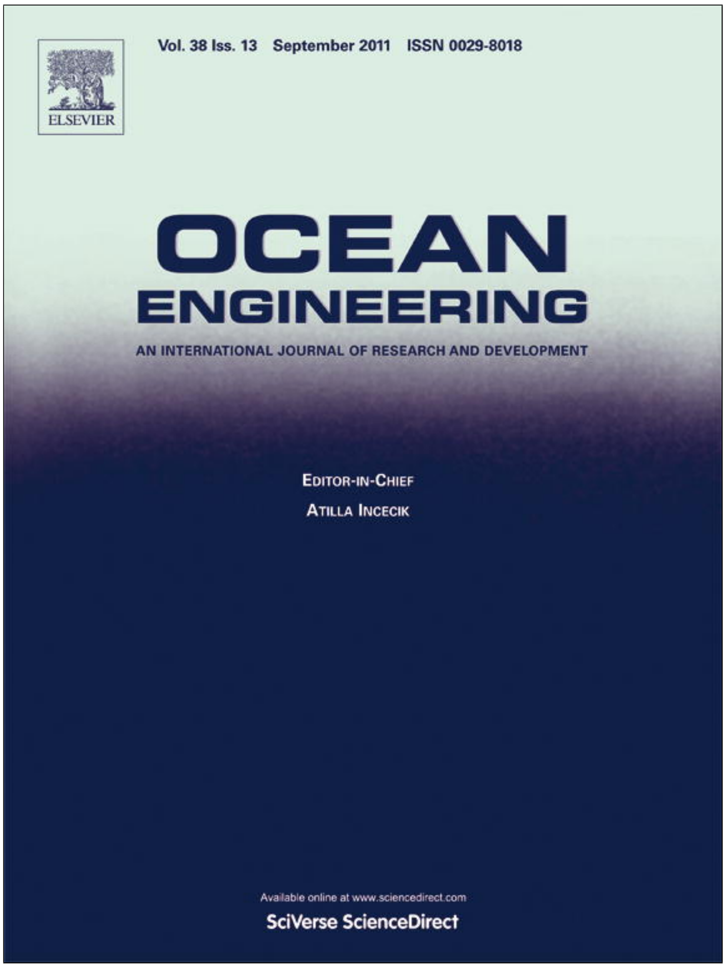
Vol. 38 Iss. 13 September 2011 ISSN 0029-8018
ELSEVIER
OCEAN
ENGINEERING
AN INTERNATIONAL JOURNAL OF RESEARCH AND DEVELOPMENT
EDITOR-IN-CHIEF
ATILLA INCECIK
Available online at www.sciencedirect.com
SciVerse ScienceDirect

Ocean Engineering 38 (2011) 1417–1429

Contents lists available at ScienceDirect

Ocean Engineering

journal homepage: www.elsevier.com/locate/oceaneng

Effect of slowly varying drift forces on the motion characteristics of truss spar platforms

O.A. Montasir *, V.J. Kurian [1]

Civil Engineering Department, Universiti Teknologi PETRONAS, 31750 Tronoh, Perak Darul Ridzuan, Malaysia

ARTICLE INFO

Article history:
Received 27 August 2010
Accepted 10 July 2011
Editor-in-Chief: A.I. Incecik
Available online 3 August 2011

Keywords:
Truss spar
Second order drift forces
Quasi-static analysis
Time domain analysis
Numerical integration

ABSTRACT

Spar platform has been regarded as a competitive floating structure for deep and ultra deep water oil and gas production. In this paper, an efficient methodology has been developed to determine the slow motion responses of slender floating offshore structures due to wave forces. Based on this methodology, a MATLAB program named 'TRSPAR' was developed to predict the dynamic responses in time domain and it was used in this study to obtain the numerical results of a typical truss spar platform connected to sea bed using nine taut mooring lines. The difference frequency forces were calculated using the principles of the extension of Morison equation for an inclined cylinder and the wave kinematics were predicted using hyperbolic extrapolation. Mooring lines were modelled as nonlinear springs and their stiffness was obtained by conducting the static offset simulation. Because of the lack of detailed calculations in literature, most of the equations used were derived and presented in this paper. The effects of the different sources of the second order difference frequency forces were compared for inertia and drag forces in terms of response spectra. To validate the TRSPAR code, its results were compared to results of a typical truss spar model test.

1. Introduction

As offshore oil and gas exploration and production are going into ultra deep water, many innovative floating offshore structures are being proposed for cost savings. One of these innovations is spar platform. Although the concept is not new (Rudnick, 1964, 1967), it has been recently the subject of renewed interest. Spars can be more economical in deep water than TLPs, they are insensitive to the deck load (Perryman and Beynet, 1994), and they can be relocated regardless of the number of wells or the water depth. Recently truss spar platforms, which are significantly modified from the conventional classic spar platforms, are becoming more popular. The conventional spar has a long circular cylinder hull, whereas the truss spar consists of an upper circular tank, a middle truss part with some horizontal plates and a lower ballast tank at the keel. Because these two types of spars are quite different in shape, their motion characteristics are also quite different.

The spar is designed to have natural periods of vibration much higher than the dominant wave periods, so that there are hardly any linear forces at the natural frequencies. Due to the nature of nonlinear surface water waves, the difference frequency interactions among ocean wave components may result in low frequency wave excitation forces. Although the nonlinear low frequency wave forces are small in magnitude, the structure, however, may experience large low frequency motions, known as slow drift motions, because the exciting frequency is close to the natural frequency.

The research interest on spars has evolved recently and within a short period several researchers have investigated the dynamic response of spars numerically as well as experimentally. Most of the previous studies on the second order forces were applied to the first generation spar, namely classic spar.

A study by a Joint Industry Project (Johnson, 1995) showed that the responses of spar buoy at the wave frequency, even near the spectrum peak frequency, were small but relatively large near its natural frequencies, although elevation measurements showed that the incident waves had insignificant energy at these low frequencies. Several studies demonstrated the importance of these second order forces. Mekha et al. (1995, 1996) studied the behaviour of spar in deep water. In their work, they applied two different methods to calculate the wave forces in time domain considering several second order effects. They also investigated the effect of modelling the mooring lines as nonlinear spring. Diffraction theory and boundary elements were used by Ran et al. (1996) to study the behaviour of spar in time domain using second order difference frequency wave loads. This was further

* Corresponding author. Tel.: +601 75701471.
E-mail addresses: montaserageeb@yahoo.com (O.A. Montasir), kurian_john@petronas.com.my (V.J. Kurian).
[1] Tel.: +605 3687345.

0029-8018/$ - see front matter © 2011 Elsevier Ltd. All rights reserved.
doi:10.1016/j.oceaneng.2011.07.007

enhanced by Ran and Kim (1997) and Ran et al. (1998), who executed a nonlinear coupled dynamic analysis of a moored spar in random waves with and without current in both time and frequency domains.

A new methodology was developed by Cao and Zhang (1996) to predict slow drift responses of slender compliant offshore structures due to ocean waves. They used hybrid wave model (Zehang et al., 1995) and the Morison equation to predict the wave kinematics and wave forces respectively for irregular waves. Hybrid wave model is different from the other approaches by decomposition of the observed wave elevation into 'free' waves up to second order accuracy while the conventional methods consider the wave elevations to be only linear combinations of individual sinusoids.

In this paper, a quasi-static cable analysis was conducted in order to obtain the tension-displacement characteristics of the mooring system. This study addresses the effect of the difference frequency forces on the dynamic responses of truss spar using an efficient numerical scheme for predicting the first and second order dynamic responses of typical floating offshore structures. In addition, the paper includes a comparison between numerical and experimental results for validating the numerical scheme.

2. Theoretical formulation and numerical scheme

2.1. Governing equations

One of the most useful theories in calculating the kinematics of a progressive wave (Fig. 1) is linear airy theory (LAT), which is based on the assumption that the wave height (H) is small compared to the wave length (L) or water depth (d). This assumption allows the free surface boundary conditions to be linearized by dropping wave height terms which are beyond the first order and also to be satisfied at the mean water level (MWL), rather than at the oscillating free surface. For unidirectional regular waves, the first order velocity potential is given by

$$\phi^{(1)} = \frac{ag}{\omega}\frac{\cosh ks}{\cosh kd}\sin\theta \tag{1}$$

where g is the gravity acceleration. ω, k and a are the wave frequency, wave number and wave amplitude, respectively.

$$\theta = kx - \omega t + \beta$$

where β is the initial phase angle.

The wave elevation is

$$\eta = \frac{H}{2}\cos\theta \tag{2}$$

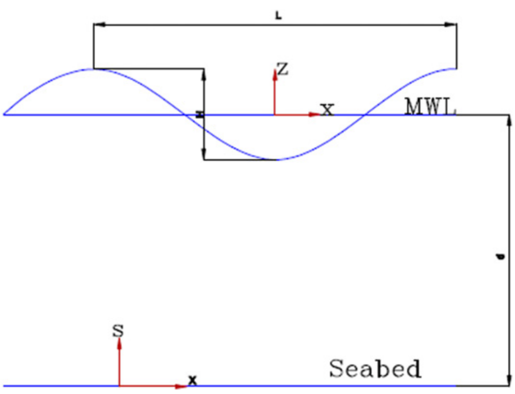

Fig. 1. Definition sketch for a progressive wave train.

The water-particle velocities and accelerations in the x and z directions are

$$u = \frac{H}{2}\omega\frac{\cosh ks}{\sinh kd}\cos\theta \tag{3}$$

$$v = \frac{H}{2}\omega\frac{\sinh ks}{\sinh kd}\sin\theta \tag{4}$$

$$\frac{\partial u}{\partial t} = \frac{H}{2}\omega\frac{\cosh ks}{\sinh kd}\sin\theta \tag{5}$$

$$\frac{\partial v}{\partial t} = -\frac{H}{2}\omega\frac{\sinh ks}{\sinh kd}\cos\theta \tag{6}$$

For random waves, these equations apply to each wave component in order to get the resultant wave kinematics by adding up the individual effects from all wave components.

In this study, hyperbolic extrapolation is used. It is based on the assumption that the wave kinematics between the MWL and free surface follow the same LAT hyperbolic variations with depth as they do up to the MWL.

The wave forces are decomposed into two components; normal and tangential to the structure. The preceding component is calculated using an extension of the Morison equation for an inclined cylinder, which is based upon normal velocities and accelerations as shown in Fig. 2

$$u_x = u - C_x(C_x u + C_z v)$$
$$u_z = v - C_z(C_x u + C_z v) \tag{7}$$

where C_x, C_z are x and z components, respectively, of the unit vector C, which is acting along the cylinder axis directed up or down.

Two coordinate systems are illustrated in Fig. 3, the global axis (xoz) is fixed at MWL and the local axis ($\zeta G\eta$) is fixed on the centre of gravity of the structure.

The normal wave force per unit length can be written as

$$f = \rho C_M A\frac{\partial w}{\partial t} + \frac{1}{2}\rho C_D D|w|w + \rho C_m A w \tau^T V \tau \tag{8}$$

where ρ is the mass density of wave. C_M, C_D and C_m are the inertia, drag and added mass coefficients, respectively. A and D are the cross-sectional area and structure diameter, respectively. w is the relative normal velocity.

$$\tau = \begin{bmatrix}\sin\vartheta \\ \cos\vartheta\end{bmatrix}$$

where ϑ is the pitch angle.

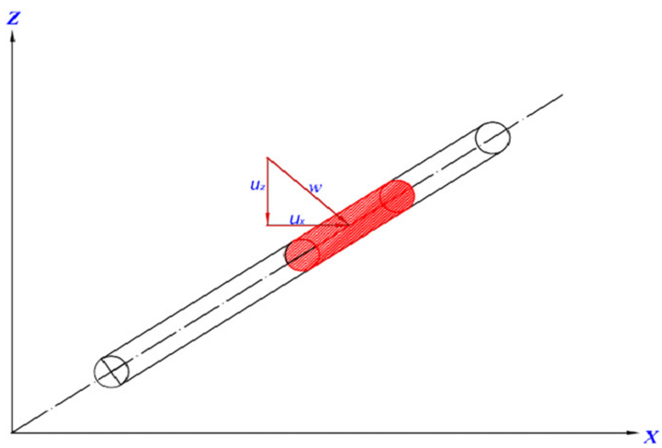

Fig. 2. Wave kinematics components on a segment on inclined cylinder.

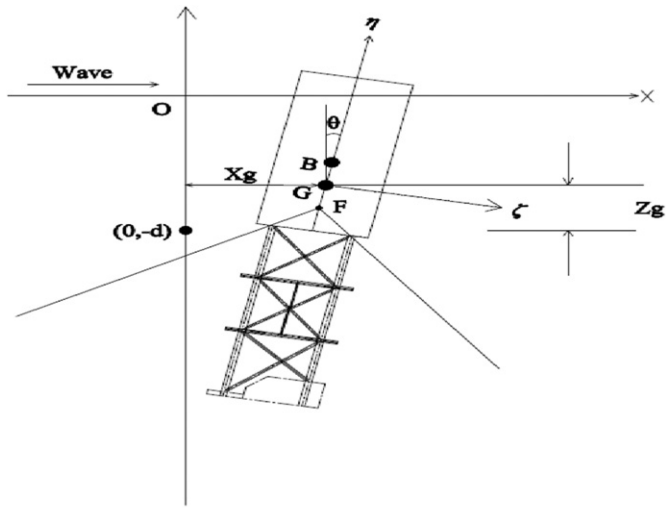

Fig. 3. Global and local coordinates used for dynamic analysis.

The last term in Eq. (8) represents the normal axial divergence in which the velocity gradient matrix is given by

$$V=\begin{bmatrix}\frac{\partial u}{\partial x} & \frac{\partial u}{\partial z}\\ \frac{\partial v}{\partial x} & \frac{\partial v}{\partial z}\end{bmatrix} \tag{9}$$

The tangential component is predicted by carrying out a double integration of the dynamic pressure on the bottom surface of the structure B, which is derived from the Bernoulli equation and the potential velocity.

$$F_{Ext}=\iint\left[\rho g a\frac{\cosh(ks)}{\cosh(kd)}\cos\theta+\frac{3}{4}\rho g\frac{\pi H^2}{L}\frac{1}{\sinh(2kd)}\left[\frac{\cosh 2ks}{\sinh^2 kd}-\frac{1}{3}\right]\cos 2\theta -\frac{1}{4}\rho g\frac{\pi H^2}{L}\frac{1}{\sinh 2kd}\left[\cosh 2ks-1\right]\right]\partial B \tag{10}$$

2.2. Second order wave forces

The potential velocity for the interaction between the wave components within a random wave was derived up to the second order by Longuet-Higgins and Steward (1960) using a conventional perturbation approach

$$\varphi=\sum\left\{A_i\frac{\cosh(k_is)}{\cosh(k_id)}\sin\theta_i+A_{ii}\frac{\cosh(2k_is)}{\sinh^4(k_id)}\sin 2\theta_i\right\} +\sum\sum\left\{A_{i-j}\frac{\cosh[(k_i-k_j)\,s]}{\cosh[(k_i-k_j)\,d]}\sin(\theta_i-\theta_j) +A_{i+j}\frac{\cosh[(k_i+k_j)s]}{\cosh[(k_i+k_j)d]}\sin(\theta_i+\theta_j)\right\} \tag{11}$$

where the first Σ indicates a summation over ith waves and the second Σ is a summation over jth interacting waves for $\omega_i>\omega_j$ only.

Also $A_{ii}=3a_i{}^2\omega_i/8$ (12)

$$\lambda=\omega_j/\omega_i \tag{13}$$

$$\alpha_i=\coth(k_id) \tag{14}$$

$$A_{i-j}=a_ia_j\omega_i(\alpha_i\alpha_j-1)/2[2\lambda(1-\lambda)(\alpha_i\alpha_j+1) -\lambda^3(\alpha_j{}^2-1)+\alpha_i{}^2-1]/[(\alpha_i-\lambda\alpha_j)^2-(1-\lambda)^2] \tag{15}$$

For A_{i+j}, only the signs for α_j and ω_j will be changed.

The first term in Eq. (11) represents the first order potential velocity, whereas the second, third and fourth terms stand for second order potential velocity working at a frequency twice that of the linear term, difference frequency and sum frequency, respectively.

As mentioned earlier, floating structures, like spar, have natural frequencies lower than the incident ocean wave frequencies so that the third term in Eq. (11) is the most important term in studying the effects of the second order forces on spar.

The second order difference frequency forces can be classified into five categories:

1. Structure displacement
2. Axial divergence
3. Free surface fluctuation
4. Convective acceleration
5. Temporal acceleration of the second order incident wave.

The inertia and drag forces are calculated in the structure displaced position and the effect of the free surface fluctuation are also considered. The convective acceleration is added to the first and second order temporal accelerations to obtain the total wave acceleration for the inertia force.

2.2.1. Inertia forces

Because spar platforms have low Keulegan–Carpenter parameter (KC), the contribution of drag force is small compared to the inertia force. Up to the second order, the inertia force can be written as

$$F_I=\int_{n_b}^{n_t}\rho C_MA\frac{\partial(w_{SD})}{\partial t}\cdot\partial n+\int^{\eta}\rho C_MA\frac{\partial(w_{FS})}{\partial t}\cdot\partial n +\int_{n_b}^{n_t}\rho C_MAw_{CA}\cdot\partial n+\int_{n_b}^{n_t}\rho C_MA\frac{\partial(w_{TA}^{(2)})}{\partial t}\cdot\partial n \tag{16}$$

where the first, second, third and fourth parts of Eq. (16) are for the second order difference frequency inertia forces due to the structural displacement, free surface fluctuation, convective and temporal accelerations respectively, $\int_{n_b}^{n_t}$ is the integration between the bottom and the top of the structure, and $\int^{\eta}$is the integration between MWL and the instant free surface.

2.2.1.1. Structure displacement. The forces on the structure must be calculated at the displaced position instead of at the mean position. This adds nonlinear force on the spar (Li and Kareem, 1992). The horizontal and vertical wave particle accelerations up to the second order can be written as

$$\frac{\partial u}{\partial t}=\sum a_i\omega_i^2\left[\frac{\cosh(k_is)}{\sinh(k_id)}\right]\sin\theta_i +\left[\sum\sum\left\{x_{Gim}a_j\omega_j^2k_j\left[\frac{\cosh(k_js)}{\sinh(k_jd)}\right]-x_{Gjm}a_i\omega_i^2k_i\left[\frac{\cosh(k_is)}{\sinh(k_id)}\right]\right\} +n\sum\sum\left\{\gamma_{im}a_j\omega_j^2k_j\left[\frac{\cosh(k_js)}{\sinh(k_jd)}\right]-\gamma_{jm}a_i\omega_i^2k_i\left[\frac{\cosh(k_is)}{\sinh(k_id)}\right]\right\}\right] \times\frac{\sin(\theta_i-\theta_j)}{2} \tag{17}$$

$$\frac{\partial v}{\partial t}=-\sum a_i\omega_i^2\left[\frac{\sinh(k_is)}{\sinh(k_id)}\right]\cos\theta_i +\left[\sum\sum\left\{x_{Gim}a_j\omega_j^2k_j\left[\frac{\sinh(k_js)}{\sinh(k_jd)}\right]+x_{Gjm}a_i\omega_i^2k_i\left[\frac{\sinh(k_is)}{\sinh(k_id)}\right]\right\} +n\sum\sum\left\{\gamma_{im}a_j\omega_j^2k_j\left[\frac{\sinh(k_js)}{\sinh(k_jd)}\right]+\gamma_{jm}a_i\omega_i^2k_i\left[\frac{\sinh(k_is)}{\sinh(k_id)}\right]\right\}\right] \times\frac{\cos(\theta_i-\theta_j)}{2} \tag{18}$$

where x_{Gm} and γ_m are surge and pitch amplitudes, respectively. The first term in Eqs. (17) and (18) is corresponding to the wave horizontal and vertical accelerations at the mean position while the second term is representing the nonlinear structural displacement effect. When $i=j$ Eq. (18) contributes to the mean force.

2.2.1.2. Axial divergence. Morison equation has been modified by Rainey (1989) by adding a new term to the original formula. This term, which is sometimes known as the Rainey axial divergence correction, represents a second order acceleration in addition to Morison equation. This normal acceleration is given by

$$w\tau^T V\tau = \left[\left(u-\frac{\partial x}{\partial t}\right)-C_x\left(C_x\left(u-\frac{\partial x}{\partial t}\right)+C_z\left(v-\frac{\partial z}{\partial t}\right)\right)\right]\tau^T V\tau\cos\vartheta - \left[\left(v-\frac{\partial z}{\partial t}\right)-C_z\left(C_x\left(u-\frac{\partial x}{\partial t}\right)+C_z\left(v-\frac{\partial z}{\partial t}\right)\right)\right]\tau^T V\tau\sin\vartheta \quad (19)$$

where

$$\left(u-\frac{\partial x}{\partial t}\right)\tau^T V\tau = AD_{hr1}\sin^2\vartheta+(AD_{hr2}+AD_{hrMean2})\sin\vartheta\cos\vartheta + (AD_{hr3}+AD_{hrMean3})\sin\vartheta\cos\vartheta+AD_{hr4}\cos^2\vartheta \quad (20)$$

$$AD_{hr1} = \sum\sum\omega_i\omega_j\left\{a_i a_j \frac{\cosh k_i s\cosh k_j s}{\sinh k_i d\sinh k_j d}(k_j-k_i) + a_j k_j(x_{Gim}+n\gamma_{im})\left(\left[\frac{\cosh k_j s}{\sinh k_j d}\right]\right) - a_i k_i(x_{Gjm}+n\gamma_{jm})\left(\frac{\cosh k_i s}{\sinh k_i d}\right)\right\}\frac{\sin(\theta_i-\theta_j)}{2} \quad (21)$$

$$AD_{hr2} = \sum\sum\omega_i\omega_j\left\{a_i a_j \frac{k_j\sinh k_j s\cosh k_i s+k_i\sinh k_i s\cosh k_j s}{\sinh k_i d\sinh k_j d} + a_j k_j(x_{Gim}+n\gamma_{im})\left[\frac{\sinh k_j s}{\sinh k_j d}\right] + a_i k_i(x_{Gjm}+n\gamma_{jm})\left[\frac{\sinh k_i s}{\sinh k_i d}\right]\right\}\frac{\cos(\theta_i-\theta_j)}{2} \quad (22)$$

$$AD_{hr3} = AD_{hr2} \quad (23)$$

$$AD_{hr4} = \sum\sum\omega_i\omega_j\left\{a_i a_j \frac{\cosh k_i s\cosh k_j s}{\sinh k_i d\sinh k_j d}(k_i-k_j) + a_i k_i(x_{Gjm}+n\gamma_{jm})\left(\left[\frac{\cosh k_i s}{\sinh k_i d}\right]\right) - a_j k_j(x_{Gim}+n\gamma_{im})\left(\frac{\cosh k_j s}{\sinh k_j d}\right)\right\}\frac{\sin(\theta_i-\theta_j)}{2} \quad (24)$$

$$\left(v-\frac{\partial z}{\partial t}\right)\tau^T V\tau = (AD_{vr1}+AD_{vrMean1})\sin^2\vartheta + (AD_{vr2}+AD_{vrMean2})\sin\vartheta\cos\vartheta + (AD_{vr3}+AD_{vrMean3})\sin\vartheta\cos\vartheta + (AD_{vr4}+AD_{vrMean4})\cos^2\vartheta \quad (25)$$

$$AD_{vr1} = -\sum\sum\omega_i\omega_j a_i a_j\left[\frac{\sinh k_j s}{\sinh k_j d}k_i\frac{\cosh k_i s}{\sinh k_i d}+\frac{\sinh k_i s}{\sinh k_i d}k_j\frac{\cosh k_j s}{\sinh k_j d}\right]\frac{\cos(\theta_i-\theta_j)}{2} + \sum\sum\left[a_j k_j\omega_j\frac{\cosh k_j s}{\sinh k_j d}Z_{Gim}-a_i k_i\omega_i\frac{\cosh k_i s}{\sinh k_i d}Z_{Gjm}\right]\frac{\sin(\theta_i-\theta_j)}{2} \quad (26)$$

$$AD_{vr2} = \sum\sum\omega_i\omega_j a_i a_j\frac{\sinh k_i s\sinh k_j s}{\sinh k_i d\sinh k_j d}(k_j-k_i)\frac{\sin(\theta_i-\theta_j)}{2} + \sum\sum\omega_i\omega_j\left[a_i k_i\frac{\sinh k_i s}{\sinh k_i d}Z_{Gjm}+a_j k_j\frac{\sinh k_j s}{\sinh k_j d}Z_{Gim}\right]\times\frac{\cos(\theta_i-\theta_j)}{2} \quad (27)$$

$$AD_{vr3} = AD_{vr2} \quad (28)$$

$$AD_{vr4} = \sum\sum\omega_i\omega_j a_i a_j\left[\frac{\cosh k_i s}{\sinh k_i d}k_i\frac{\sinh k_j s}{\sinh k_j d}+\frac{\cosh k_j s}{\sinh k_j d}k_j\frac{\sinh k_i s}{\sinh k_i d}\right]\frac{\cos(\theta_i-\theta_j)}{2} + \sum\sum\left[a_i k_i\omega_i\omega_j\frac{\cosh k_i s}{\sinh k_i d}Z_{Gjm}-a_j k_j\omega_i\omega_j\frac{\cosh k_j s}{\sinh k_j d}Z_{Gim}\right]\times\frac{\sin(\theta_i-\theta_j)}{2} \quad (29)$$

where Z_{Gm} is the heave amplitude. Since some of the above equations have a difference frequency cosine terms, there will be a contribution to the mean force. This will occur when $i=j$.

$$AD_{hrMean2} = \frac{1}{2}\sum\omega_i^2 a_i k_i\left[\frac{\sinh k_i s}{\sinh k_i d}\right]\left\{a_i\frac{\cosh k_i s}{\sinh k_i d}+x_{Gim}+n\gamma_{im}\right\} \quad (30)$$

$$AD_{hrMean3} = AD_{hrMean2} \quad (31)$$

$$AD_{vrMean1} = -\frac{1}{2}\sum a_i^2\omega_i^2 k_i\left[\frac{\sinh k_i s\cosh k_i s}{\sinh^2 k_i d}\right] \quad (32)$$

$$AD_{vrMean2} = \frac{1}{2}\sum a_i\omega_i^2 k_i\frac{\sinh k_i s}{\sinh k_i d}Z_{Gim} \quad (33)$$

$$AD_{vrMean3} = AD_{vrMean2} \quad (34)$$

$$AD_{vrMean4} = \frac{1}{2}\sum a_i^2\omega_i^2 k_i\frac{\sinh k_i s\cosh k_i s}{\sinh^2 k_i d} \quad (35)$$

2.2.1.3. Free surface fluctuation. The integration of the first order accelerations from the MWL to the wave free surface gives another source of the nonlinear difference frequency forces. The integration of the corresponding second order horizontal and vertical accelerations leads to

$$\int^n\frac{\partial u}{\partial t}\cdot\partial n = \sum\sum a_i a_j\frac{g}{\cos\vartheta}(k_i-k_j)\frac{\sin(\theta_i-\theta_j)}{2} \quad (36)$$

$$\int^n\frac{\partial v}{\partial t}\cdot\partial n = -\frac{g}{\cos\theta}\sum a_i a_j(k_i+k_j)\frac{\cos(\theta_i-\theta_j)}{2} \quad (37)$$

As in the axial divergence effect, there is also a contribution to the mean force when putting $i=j$ in Eq. (37)

$$\int^n\frac{\partial v}{\partial t}\cdot\partial n = -\frac{g}{2\cos\theta}\sum a_i^2 k_i \quad (38)$$

2.2.1.4. Convective acceleration. The total wave particle acceleration is due to the change of the wave particle velocity with time and space. The change with time is known as temporal acceleration while the change with space is known as convective acceleration. The horizontal and vertical wave particle convective accelerations up to the second order can be written as

$$\left(u\frac{\partial u}{\partial x}+v\frac{\partial u}{\partial z}\right) = -\sum\sum a_i a_j\omega_i\omega_j(k_i-k_j)\times\left\{\frac{\cosh(k_i+k_j)s}{\sinh k_i d\sinh k_j d}\right\}\frac{\sin(\theta_i-\theta_j)}{2} \quad (39)$$

$$\left(u\frac{\partial v}{\partial x}+v\frac{\partial v}{\partial z}\right) = \sum a_i^2\omega_i^2 k_i\left[\frac{\cosh k_i s\sinh k_i s}{\sinh^2 k_i d}\right] + \sum\sum a_i a_j\omega_i\omega_j\left\{(k_i+k_j)\left[\frac{\sinh(k_i+k_j)s}{\sinh k_i d\sinh k_j d}\right]\right\}\times\frac{\cos(\theta_i-\theta_j)}{2} \quad (40)$$

The first part of Eq. (40) contributes to the mean force. It is interesting to compare the free surface effect with the convective acceleration, using Eqs. (36), (37), (39), and (40) for this purpose, one can observe that the two forces are working opposite to each other.

2.2.1.5. Temporal acceleration. For the spar, the second order wave particle acceleration derived from the second order potential at the difference frequency due to the wave components interaction has a major part of the forces at the natural frequencies compare to the first order wave acceleration. The horizontal and vertical wave particle temporal accelerations up to the second order can be written as

$$\frac{\partial u^{(2)}}{\partial t} = \sum\sum\left\{\frac{(\omega_i-\omega_j)/(\omega_i\omega_j)k_ik_j[1+\tanh k_id\tanh k_jd]+(k_i^2\,\mathrm{sech}^2(k_id)/\omega_i-k_j^2\,\mathrm{sech}^2(k_jd)/\omega_j)/2}{g(k_i-k_j)\tanh((k_i-k_j)d)-(\omega_i-\omega_j)^2}\right\} \times a_ia_j(\omega_i-\omega_j)g^2(k_i-k_j)\left[\frac{\cosh((k_i-k_j)s)}{\cosh((k_i-k_j)d)}\right]\sin(\theta_i-\theta_j) \quad (41)$$

$$\frac{\partial v^{(2)}}{\partial t} = -\sum\sum\left\{\frac{(\omega_i-\omega_j)/(\omega_i\omega_j)k_ik_j[1+\tanh k_id\tanh k_jd]+(k_i^2\,\mathrm{sech}^2(k_id)/\omega_i-k_j^2\,\mathrm{sech}^2(k_jd)/\omega_j)/2}{g(k_i-k_j)\tanh((k_i-k_j)d)-(\omega_i-\omega_j)^2}\right\} \times a_ia_j(\omega_i-\omega_j)g^2(k_i-k_j)\left[\frac{\sinh((k_i-k_j)s)}{\cosh((k_i-k_j)d)}\right]\cos(\theta_i-\theta_j) \quad (42)$$

As in the above equations, $\partial v/\partial t^{(2)}$ will contribute to the mean force when $i=j$.

2.2.2. Drag force

In the case of inertia force dominant systems, such as spar, the system may be approximated with a reasonable accuracy as a linear system in calculating the drag force and a linearization method may be adopted.

The linear approximation for the drag force per unit length is

$$f_D = \frac{1}{2}\rho C_D D\sqrt{\frac{8}{\pi}}\sigma_{wr}w_r \quad (43)$$

where σ_{wr} is the variance of the relative normal wave particle velocity. w_r is the relative normal velocity.

$$\sqrt{\frac{8}{\pi}}\sigma_{wr}w_r = \sqrt{\frac{8}{\pi}}\Big\{[(\sigma_{ur}u_r)-C_x(C_x(\sigma_{ur}u_r)+C_z(\sigma_{vr}v_r))]\cos\vartheta -[(\sigma_{vr}v_r)-C_z(C_x(\sigma_{ur}u_r)+C_z(\sigma_{vr}v_r))]\sin\vartheta\Big\} \quad (44)$$

$$\sqrt{\frac{8}{\pi}}\sigma_{ur}u_r = \sqrt{\frac{8}{\pi}}\sqrt{\sum\left(\omega_i\left\{a_i\left[\frac{\cosh k_is}{\sinh k_id}\right]-x_{Gim}-n\gamma_{im}\right\}\right)^2/2} \times\left[\sum a_i\omega_i\left[\frac{\cosh k_is}{\sinh k_is}\right]\cos\theta_i-\sum\omega_i(x_{Gim}+n\gamma_{im})\sin\theta_i\right] \quad (45)$$

$$\sqrt{\frac{8}{\pi}}\sigma_{vr}v_r = \sqrt{\frac{8}{\pi}}\sqrt{\sum\left(\omega_i\left\{a_i\left[\frac{\sinh k_is}{\sinh k_id}\right]-Z_{Gim}\right\}\right)^2/2} \times\left[\sum a_i\omega_i\left[\frac{\sinh k_is}{\sinh k_id}\right]\sin\theta_i-\sum\omega_iZ_{Gim}\sin\theta_i\right] \quad (46)$$

In Eqs. (45) and (46) the first part contributes to the excitation force and the second part to the damping of the system. Although Eqs. (45) and (46) represent the linear approximation of the drag force, there are two sources of the second order slow varying difference frequency forces involved. One is due to the integration of the wave forces at the displaced position and the other is due to free surface fluctuation effect.

2.2.2.1. Structure displacement. Just like the inertia force, calculation of the drag force at the displaced position of the structure adds a second order term as follows:

$$\sqrt{\frac{8}{\pi}}\sigma_{ur}u_r = -\sqrt{\frac{8}{\pi}}\sqrt{\sum\left(\omega_i\left\{a_i\left[\frac{\cosh k_is}{\sinh k_id}\right]-x_{Gim}-n\gamma_{im}\right\}\right)^2/2} \times\left[\sum\sum\left\{a_i\omega_ik_i(x_{Gjm}+n\gamma_{jm})\left[\frac{\cosh k_is}{\sinh k_id}\right] +a_j\omega_jk_j(x_{Gim}+n\gamma_{im})\left[\frac{\cosh k_js}{\sinh k_jd}\right]\right\}\frac{\cos(\theta_i-\theta_j)}{2}\right] \quad (47)$$

$$\sqrt{\frac{8}{\pi}}\sigma_{vr}v_r = -\sqrt{\frac{8}{\pi}}\sqrt{\sum\left(\omega_i\left\{a_i\left[\frac{\sinh k_is}{\sinh k_id}\right]-Z_{Gim}\right\}\right)^2/2} \times\left[\sum\sum\left\{a_i\omega_ik_i(x_{Gjm}+n\gamma_{jm})\left[\frac{\sinh k_is}{\sinh k_id}\right] -a_j\omega_jk_j(x_{Gim}+n\gamma_{im})\left[\frac{\sinh k_js}{\sinh k_jd}\right]\right\}\frac{\sin(\theta_i-\theta_j)}{2}\right] \quad (48)$$

2.2.2.2. Free surface fluctuation. As for the inertia force, there is an important source of the second order difference frequency forces coming from the integration of the linearized drag force up to the free surface. The expression up to the second order is

$$F_D^{FS} = \sqrt{\frac{8}{\pi}}\rho C_D\frac{D}{2\sqrt{2}}\sqrt{\sum\left\{\omega_i\left(\frac{a_i}{\tanh k_id}-x_{Gim}-\gamma_{im}\right)\right\}^2} \times\sum\sum a_ia_j\left(\frac{\omega_i}{\tanh k_id}+\frac{\omega_j}{\tanh k_jd}\right)\frac{\cos(\theta_i-\theta_j)}{2} \quad (49)$$

2.2.2.3. Mean drag force. As for the inertia force, there will be a contribution to the mean force when $i=j$ in Eqs. (47) and (49). These equations for the mean force can be written as

$$\sqrt{\frac{8}{\pi}}\sigma_{ur}u_r = -\frac{1}{2}\sqrt{\frac{8}{\pi}}\sqrt{\sum\left(\omega_i\left\{a_i\left[\frac{\cosh k_is}{\sinh k_id}\right]-x_{Gim}-n\gamma_{im}\right\}\right)^2/2} \times\sum\left\{a_i\omega_ik_i(x_{Gim}+n\gamma_{im})\left[\frac{\cosh k_is}{\sinh k_id}\right]\right\} \quad (50)$$

$$F_{D(mean)}^{FS} = \sqrt{\frac{8}{\pi}}\rho C_D\frac{D}{2\sqrt{2}}\sqrt{\sum\left\{\omega_i\left(\frac{a_i}{\tanh k_id}-x_{Gim}-\gamma_{im}\right)\right\}^2} \sum a_i^2\left(\frac{\omega_i}{\tanh k_id}\right)/2 \quad (51)$$

2.3. Numerical integration approach

All the above equations are incorporated in a MATLAB program named 'TRSPAR' for calculating the wave forces. Newmark-beta integration scheme was adopted to solve the equations of motion

$$\{M\}\left[\frac{\partial^2 x_G}{\partial t^2}\right]+\{C\}\left[\frac{\partial x_G}{\partial t}\right]+\{K\}[x_G]=[F(t)] \quad (52)$$

where $\{M\}$ is made up of body mass and added mass components as given in Eq. (53) and $[\partial^2 x_G/\partial t^2]$is the structural acceleration vector. The resultant force can be defined as

$$\{M\}\left[\frac{\partial^2 x_G}{\partial t^2}\right] = \left\{\underbrace{\begin{bmatrix} m & 0 & 0\\ 0 & m & 0\\ 0 & 0 & I\end{bmatrix}}_{\text{Mass matrix}}+\underbrace{\begin{bmatrix} m_{11} & m_{12} & m_{13}\\ m_{21} & m_{22} & m_{23}\\ m_{31} & m_{32} & m_{33}\end{bmatrix}}_{\text{Added mass matrix}}\right\}\begin{bmatrix}\frac{\partial^2 x_G}{\partial t^2}\\ \frac{\partial^2 z_G}{\partial t^2}\\ \frac{\partial^2 \vartheta}{\partial t^2}\end{bmatrix} \quad (53)$$

where m and I denote body mass and mass moment of inertia about the y-axis, respectively. The added mass is determined by integrating the added mass from the bottom of the structure/member to the instantaneous surface elevation. The computations of added mass forces and moments are as follows:

$$m_{11} = \int_{n_b}^{n_t} \rho C_m A \cdot \partial n \cos\vartheta \cos\vartheta$$

$$m_{12} = m_{21} = -\int_{n_b}^{n_t} \rho C_m A \cdot \partial n \sin\vartheta \cos\vartheta$$

$$m_{13} = m_{31} = \int_{n_b}^{n_t} \rho C_m A n \cdot \partial n \cos\vartheta$$

$$m_{22} = \int_{n_b}^{n_t} \rho C_m A \cdot \partial n \sin\vartheta \sin\vartheta$$

$$m_{23} = m_{32} = -\int_{n_b}^{n_t} \rho C_m A n \cdot \partial n \sin\vartheta$$

$$m_{33} = \int_{n_b}^{n_t} \rho C_m A n^2 \cdot \partial n \tag{54}$$

$\{C\}[\partial x_G/\partial t]$ is the structure damping matrix multiply by body velocity vector in the considered degrees of freedom. The resultant force can be defined as

$$\{C\}\left[\frac{\partial x_G}{\partial t}\right] = \begin{bmatrix} c_{11} & 0 & 0 \\ 0 & c_{22} & 0 \\ 0 & 0 & c_{33} \end{bmatrix} \begin{bmatrix} \frac{\partial x_G}{\partial t} \\ \frac{\partial z_G}{\partial t} \\ \frac{\partial \vartheta}{\partial t} \end{bmatrix} \tag{55}$$

Damping sources can be identified as structural, radiation, wave drift and mooring lines. The significant contribution comes from the drag force on the truss spar when using the Morison equation as mentioned in Section 2.2.2. The structure damping of the system is small compared to the other forces. That is due to the low natural frequencies of the system in all degrees of freedom. The computations of the structure damping elements are as follows:

$$c_{11} = 2\xi_s \omega_{ns} m$$

$$c_{22} = 2\xi_h \omega_{nh} m$$

$$c_{33} = 2\xi_p \omega_{np} I \tag{56}$$

where the subscripts s, h and p stand for surge, heave and pitch, respectively, ξ is the damping ratio in the specified direction of motion and ω_n is the natural frequency of the system in the specified degree of freedom. Wave drift damping can be added to the C matrix as

$$\{C\} = \begin{bmatrix} c_{11} + B_{11_{wd}} & 0 & -z_G \times B_{11_{wd}} \\ 0 & c_{22} & 0 \\ -z_G \times B_{11_{wd}} & 0 & z_G^2 \times B_{11_{wd}} \end{bmatrix} \tag{57}$$

where z_G is z-coordinate of the centre of gravity.

$$\begin{aligned} B_{11wd} &= 2.6\rho R a^2 \omega (\mathrm{kR})^2, \quad \text{when}(\mathrm{kR}) < 1 \\ &= 2.6\rho R a^2 \omega, \quad \text{otherwise} \end{aligned} \tag{58}$$

where (kR) is the diffraction parameter.

In addition to the aforementioned damping, heave plates greatly increase the heave added mass and viscous damping as follows:

$$F = \frac{1}{2}\rho U|U|L^2 C_D + \rho \frac{\partial U}{\partial t} L^3 C_A \tag{59}$$

where C_D and C_A are drag and added mass coefficients for the heave plates, respectively. U and $\partial U/\partial t$ represent the velocity and acceleration, respectively, of the plate perpendicular to its plane.

$\{K\}[x_G]$ is the system stiffness matrix multiplied by displacement vector. The stiffness matrix is composed of two main components, hydrostatic and mooring line stiffness matrices. The mooring lines, which are represented here by linear/nonlinear massless springs attached at the spar fairleads, are the only source of stiffness in the direction of surge motion. The hydrostatic buoyancy force provides the heave restoring force. Both types of stiffness contribute to the pitch stiffness. The resultant restoring force can be defined as

$$\{K\}[x_G] = \left[\underbrace{\begin{bmatrix} 0 & 0 & 0 \\ 0 & k_2 & 0 \\ 0 & 0 & k_3 \end{bmatrix}}_{\text{Hydrostatic}} + \underbrace{\begin{bmatrix} k_x & 0 & k_x h_2 \\ 0 & 0 & 0 \\ k_x h_2 & 0 & k_x h_2^2 \end{bmatrix}}_{\text{Mooring lines}} \right] \begin{bmatrix} x_G \\ z_G \\ \vartheta \end{bmatrix} \tag{60}$$

where $k_2 = \pi\rho g\,(D/2)^2$, $k_3 =$ buoyancy force $\times$ distance from G to B, $k_x =$ horizontal spring stiffness, $h_2 =$ distance from G to fairlead, In general, k_x is a nonlinear function of the structure displacements. Thus the solution process involves updating the K matrix for each new displacement.

3. Numerical results and discussions

A numerical simulation for a typical truss spar, as shown in Fig. 4, with nine mooring lines was conducted. The physical characteristics of the structure and the characteristics of the mooring lines are summarized in Tables 1 and 2 respectively.

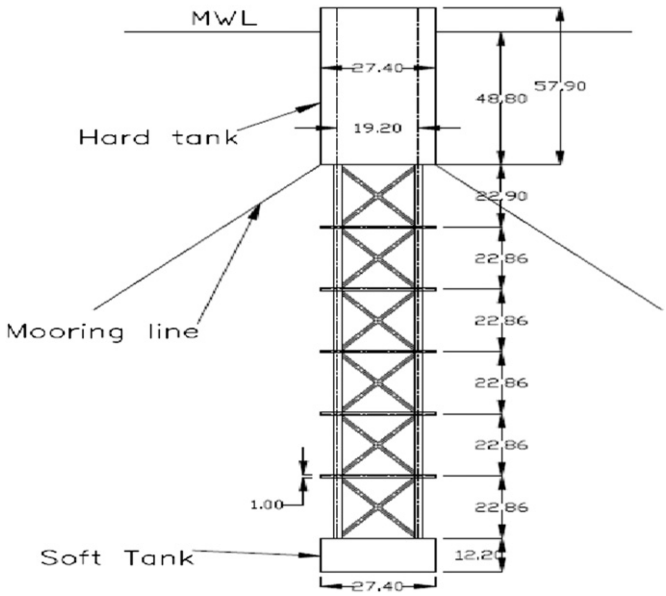

Fig. 4. Overall spar configuration (all dimensions are in m).

Table 1
Physical characteristics of the truss spar.

Weight	389.80 ton
Vertical centre of gravity (KG)	126.34 m
Buoyancy, basic	389.80 ton
Vertical centre of buoyancy (KB), basic	152.4 m
Radius of gyration for pitch	86.2 m

Table 2
Characteristics of mooring lines.

Type	Upper section K4 chain	Middle section K4 chain	Lower section K4 chain
Size (m)	0.124	0.124	0.124
Length (m)	76.2	1828.8	45.7
Wet weight (kg/m)	280.5	65.4	280.5
Eff. modulus EA (Kn)	665.9	133.9	858.9
Breaking strength (Kn)	131.9	124.6	131.9

3.1. Quasi-static simulation

A separate MATLAB program was developed to perform a quasi-static simulation for mooring line system by applying variable static forces at the fairlead. As a result, mooring stiffness curve was obtained, as shown in Fig. 5. The figure shows that the mooring line system provides nonlinear stiffness to the structure. Moreover, mooring lines restoring force caused by positive

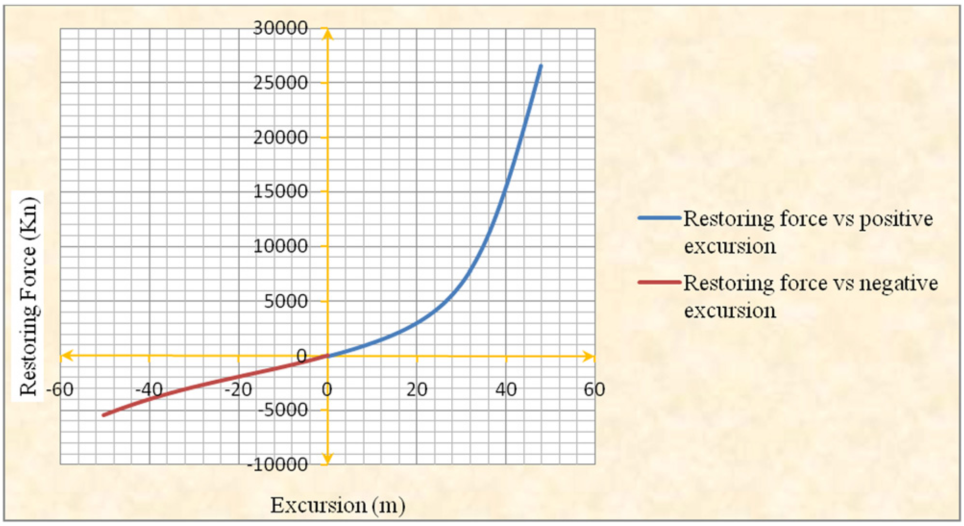

Fig. 5. Quasi-static simulation: restoring force vs. horizontal excursion.

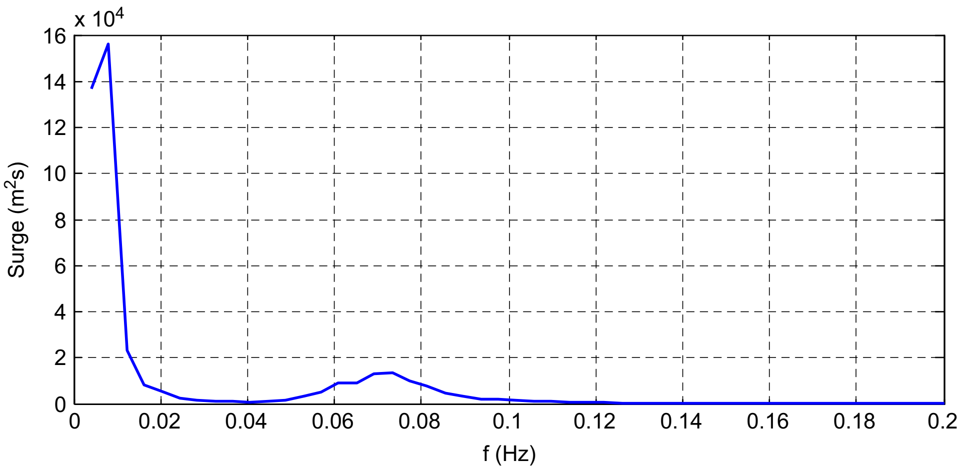

Fig. 6. Surge spectra: mean position (MP)+structure displacement (SD)+drag force (DF).

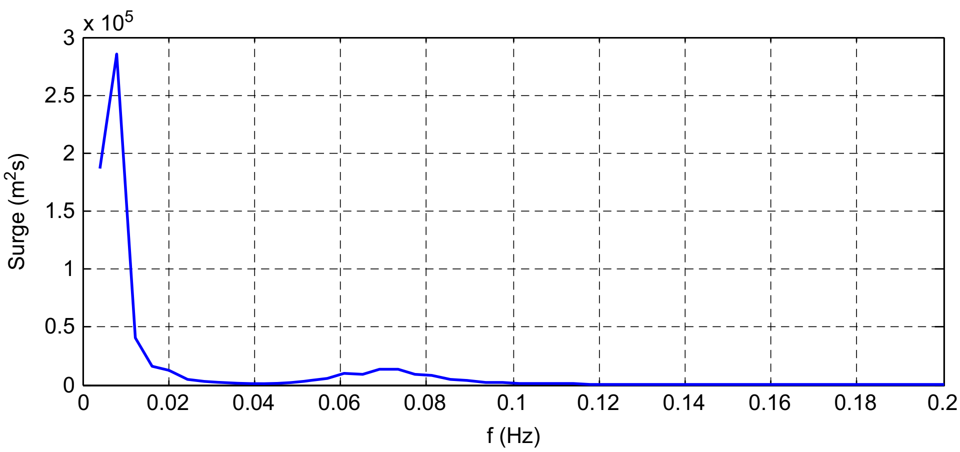

Fig. 7. Surge spectra: MP+SD+DF+axial divergence (AD).

horizontal excursion, which was in the same direction of the waves, was higher than those due to negative surge motion particularly in relatively high horizontal transient response.

3.2. Time domain simulation

Numerical studies were made using TRSPAR which included almost all the nonlinear effects up to the second order. The wave series considered here was simulated from the 100-year JONSWAP spectrum with a significant wave height of 13 m and a peak wave period of 14 s. The individual effects of the nonlinear difference frequency wave forces were examined and compared in terms of response spectra.

3.2.1. Surge response

The results, which are shown in Figs. 6–10, represent five stages corresponding to the addition of individual nonlinear

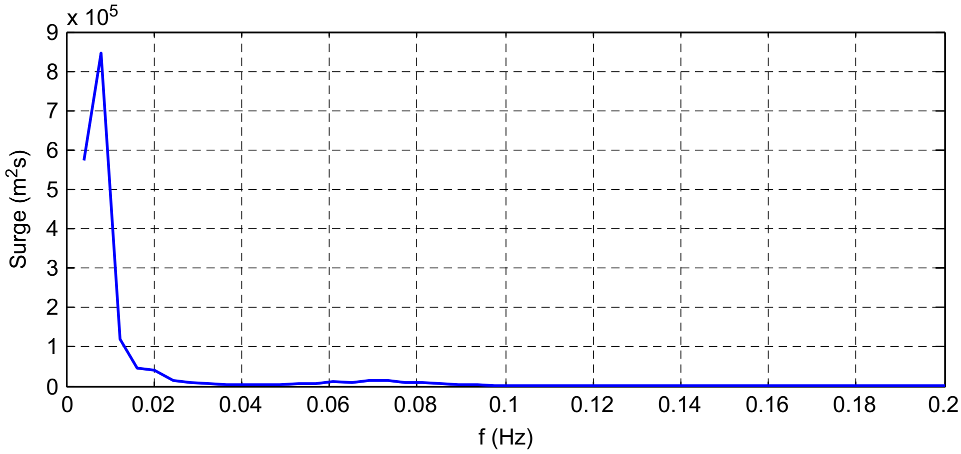

Fig. 8. Surge spectra: MP+SD+DF+AD+free surface fluctuation (FS).

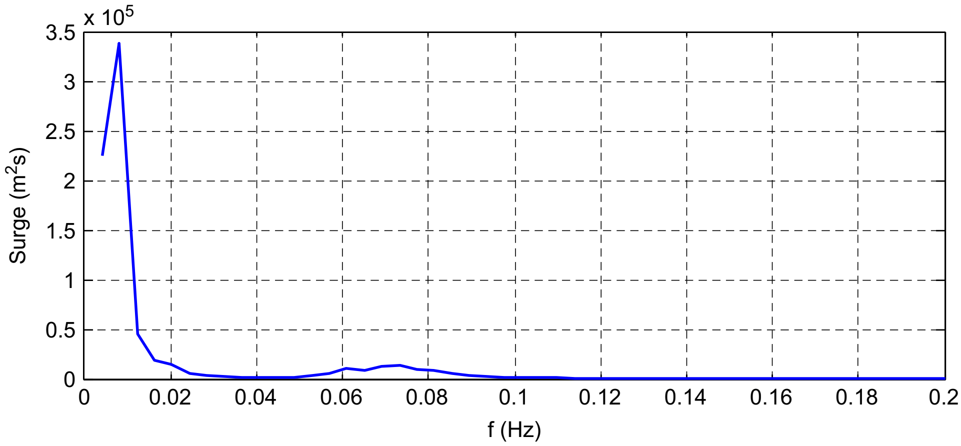

Fig. 9. Surge spectra: MP+SD+DF+AD+FS+convective acceleration (CA).

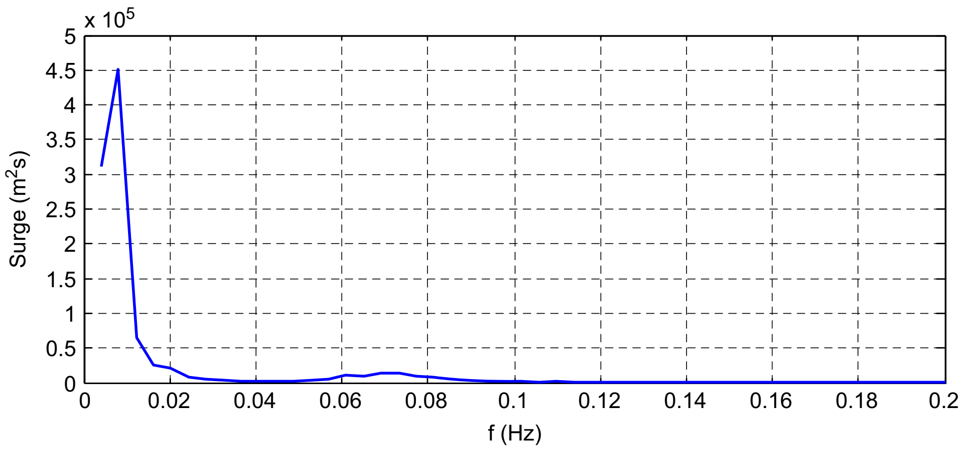

Fig. 10. Surge spectra: MP+SD+DF+AD+FS+CA+temporal acceleration (TA).

forces. It was observed that, in all figures, slowly varying surge responses were dominant. Moreover, the wave frequency surge responses did not change much throughout the addition process and hence the discussions are focused only on the second order responses. These low frequency surge responses were caused by the interactions between the wave components among the random wave.

Fig.6 represents the first stage of the process, which combined the calculation of the wave forces at the mean position with the effect of the structure displacement and the linearized drag force, which contributes to the damping of the system. In Fig. 7, where the axial divergence was added, the response increased from 1.56×10^5 to 2.85×10^5 m^2 s. The addition of free surface fluctuation in Fig. 8 shows that the response greatly increased to

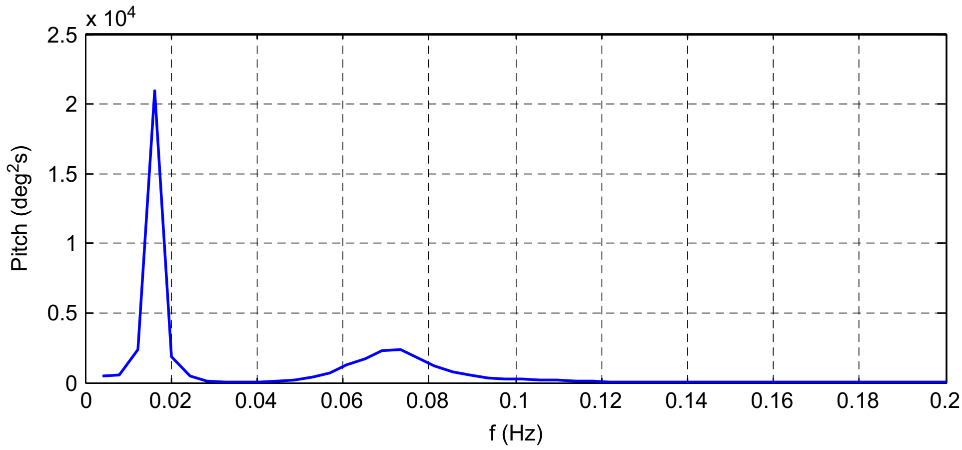

Fig. 11. Pitch spectra: MP+SD+DF.

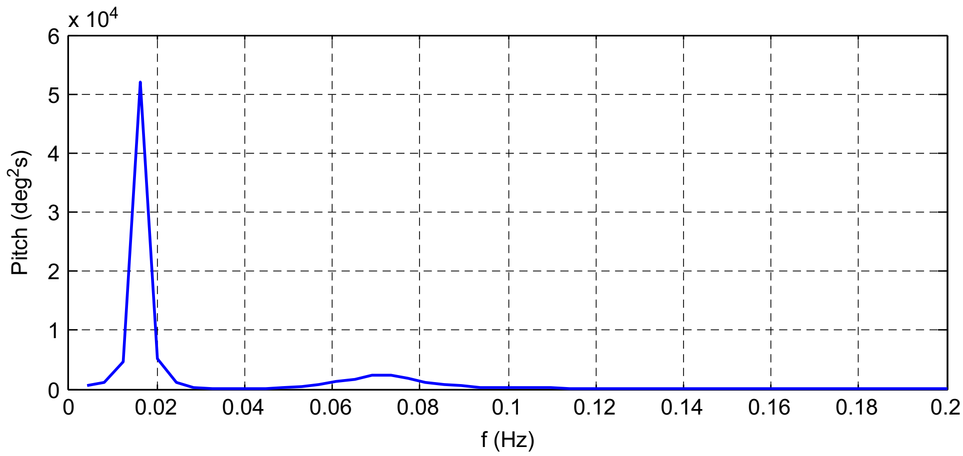

Fig. 12. Pitch spectra: MP+SD+DF+AD.

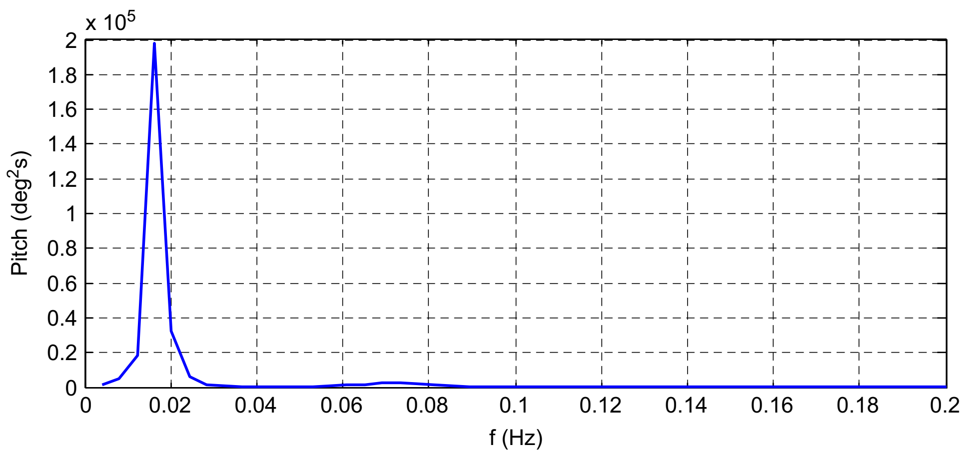

Fig. 13. Pitch spectra: MP+SD+DF+AD+FS.

8.45×10^5 m^2 s. In Fig. 9, by adding the second order convective acceleration, the surge response reduced to 3.385×10^5 m^2 s. This also agreed with Eqs. (36), (37), (39) and (40), which state that the free surface and convective acceleration effects act opposite to each other. Moreover, the effect of the free surface was more than the effect of the convective acceleration. Finally the second order temporal acceleration was added, as shown in Fig. 10. Also the surge spectra increased and reached 4.5×10^5 m^2 s.

3.2.2. *Pitch response*

The results for pitch response are shown in Figs. 11–15 in a way similar to the one used for the study with surge motion. As in surge response, slowly varying pitch responses were dominant. Also, the wave frequency pitch responses did not vary much during the addition process, hence the discussion will focus only on the second order responses.

As shown in Fig. 11, pitch response due to the combined effect of calculation of the wave forces at the mean position with the effect of the structure displacement and the linearized drag force reached 2.1×10^4 deg^2 s. In Fig. 12, pitch response was increased to 5.2×10^4 deg^2 s because of adding the axial divergence. Similar to surge motion, adding the free surface fluctuation, as shown in Fig. 13, magnify pitch response which reached 1.98×10^5 deg^2 s. Convective acceleration in Fig. 14 performs as in surge motion and reduced the pitch response to 1.12×10^5 deg^2 s. Finally the second order temporal acceleration was added, as shown in Fig. 15. Also the pitch spectra increased and reached 1.588×10^5 deg^2 s.

4. Comparison with experimental data

To validate the developed numerical scheme, a comparison between numerical results and the corresponding experimental data was conducted for the typical truss spar shown in Fig. 16. The experimental studies, which were carried out at the FORCE Technology basin are related to Kikeh project dry tree unit (Technip Document, 2005). The model scale used was 1–60.

Fig. 17 shows the truss spar model at FORCE Technology basin. The total weight of the prototype was 54×10^3 ton. The truss consisted of three bays and a box like soft tank with a length of 10.7 m. There were two heave plates with openings for the risers and strakes with cut-outs for mooring lines and transportation.

The prototype mooring system consisted of ten mooring lines in four groups. The mooring coordinate system is shown in Fig. 18 and the fairleads are located 5.5 m above the hard tank bottom. Mooring line characteristics and corresponding prototype pretension are given in Tables 3 and 4, respectively. In model test, four mooring lines consisting of length of chain and springs were used. Each mooring line represents the stiffness of a corresponding mooring group in the prototype.

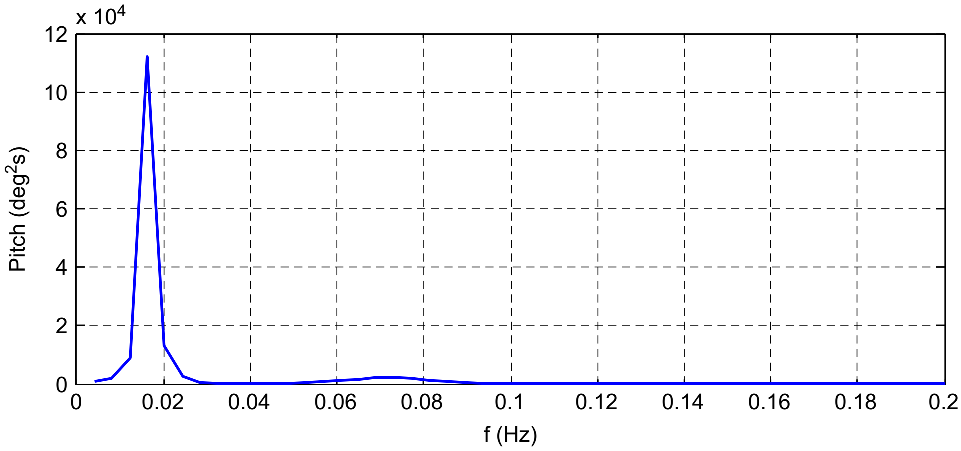

Fig. 14. Pitch spectra: MP+SD+DF+AD+FS+CA.

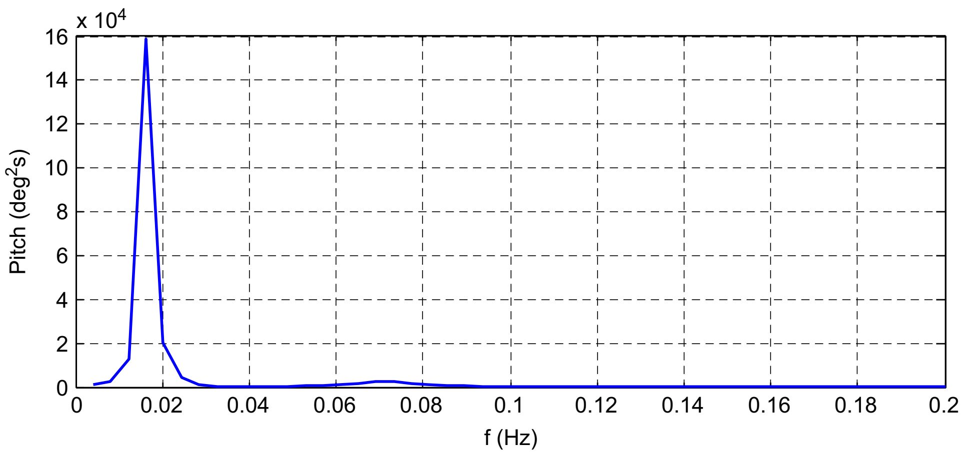

Fig. 15. Pitch spectra: MP+SD+DF+AD+FS+CA+TA.

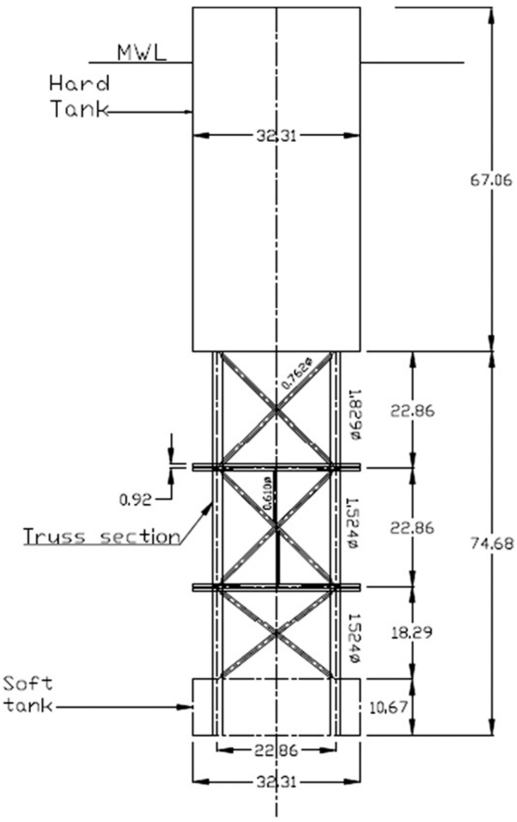

Fig. 16. Overall configuration of a typical truss spar platform (all dimensions are in m).

Fig. 17. A typical truss spar model at FORCE Technology.

Figs. 19–21 show the comparison between the measured Fourier amplitude spectra (FAS) of the model tests and those predicted by TRSPAR, which included all the nonlinear second order slowly varying wave forces. These results are for surge, heave and pitch responses due to random wave with a significant wave height of 6 m and a peak period of 11.7 s. In general, there are good agreement between the predicted and the corresponding measured results in both regions, namely wave frequency and low frequency regions. The fairly small differences between these results might be caused by the strakes and risers contributions which were modelled in the model test, but not in TRSPAR.

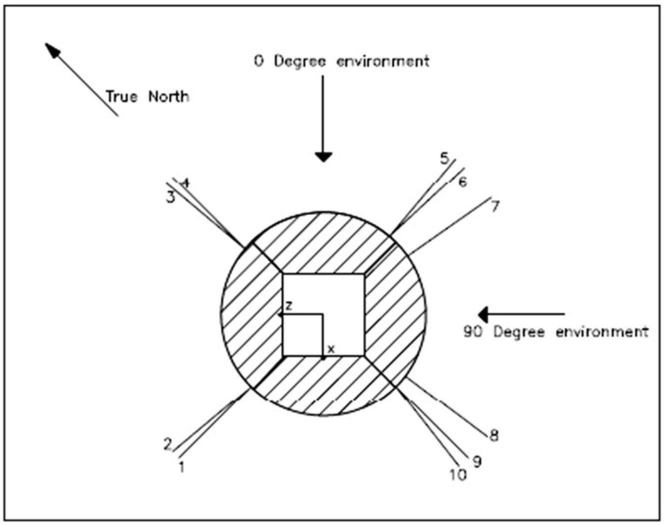

Fig. 18. Prototype spar mooring configuration.

Table 3
Truss spar prototype mooring line properties.

Spar mooring	Prototype
Platform/anchor chain	
Type	R4 Studless
Diameter	12.4 cm
Wet weight	277 Kg/m
Wire rope	
Type	Spiral strand
Diameter	10.8 cm
Wet weight	48.2 Kg/m

5. Conclusions

According to the numerical study performed on the truss spar platform, the following conclusions can be drawn:

1. An efficient methodology was developed to conduct a dynamic analysis for floating offshore structures. This methodology takes care of the inclination of the structure during the dynamic analysis using the extension of the Morison equation for an inclined cylinder for predicting the wave forces and hyperbolic extrapolation for calculating the wave kinematics.
2. Due to the lack of detailed analysis procedure in literature, the equations used for determine the slow varying difference frequency wave forces are derived and presented in this paper.

Table 4
Truss spar prototype mooring line pretensions.

Line No.	1	2	3	4	5	6	7	8	9	10
Pretension (Kn)	1610	1687	1640	1715	1210	1212	1238	1030	1015	1020

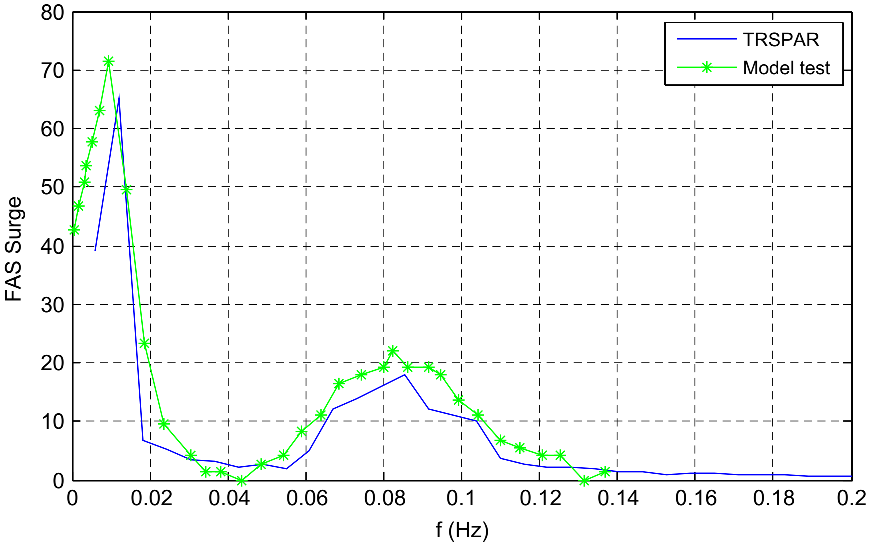

Fig. 19. FAS of the surge response comparison.

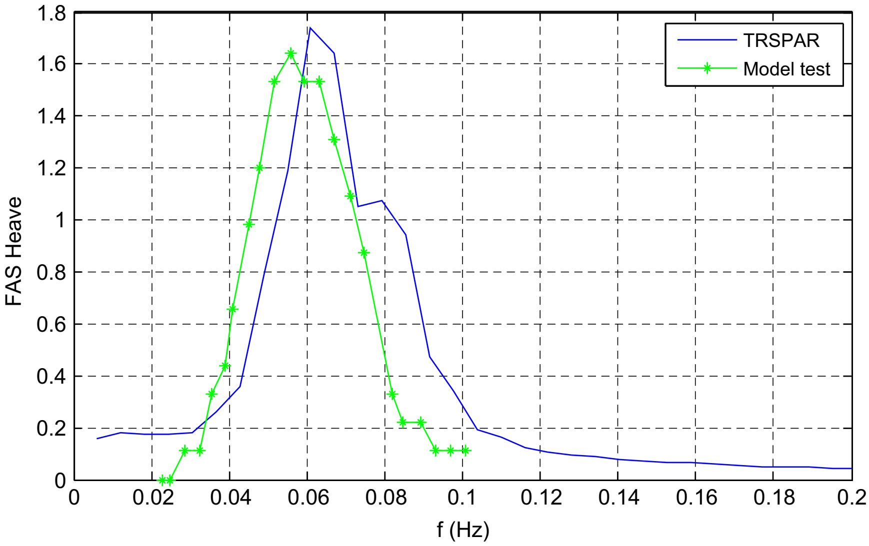

Fig. 20. FAS of the heave response comparison.

3. A MATLAB program namely 'TRSPAR', which based upon the above methodology, was developed to determine the dynamic responses of truss spar platform. This numerical model includes almost all the nonlinear effects up to the second order.
4. A separate MATLAB program using quasi-static analysis was developed to predict the stiffness of mooring lines. From the results, mooring line system shows nonlinear behaviour. It was shown that the restoring force caused by positive horizontal excursion was higher than those due to negative surge motion particularly in relatively high surge motion.
5. Surge and pitch motion results showed that the second order responses were dominant and the wave frequency motions hardly changed throughout the study.
6. Except for the convective acceleration, all other second order effects contributed positively to the surge and pitch motions. It was shown that the magnitude of the convective acceleration is almost equal to the magnitude of the free surface fluctuation.
7. A model test correlation with TRSPAR has been made. The measured results agree with the corresponding predictions. This implies that the developed numerical scheme is capable

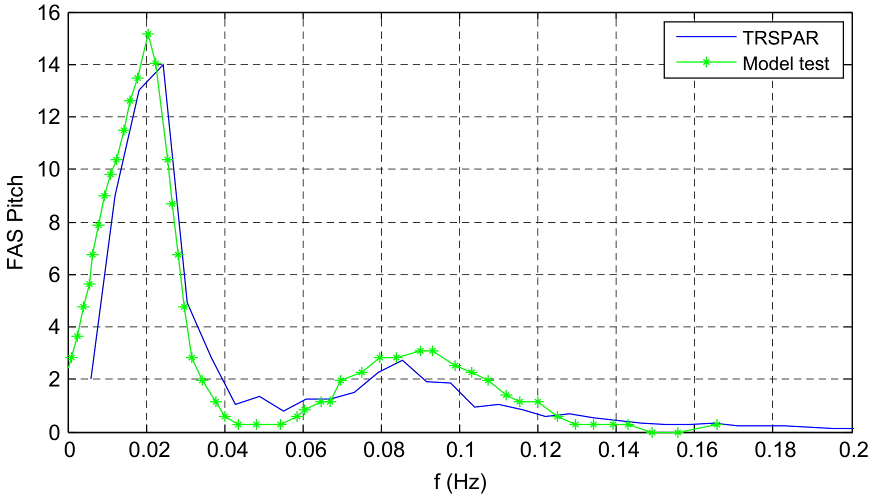

Fig. 21. FAS of the pitch response comparison.

of accurately predicting the dynamic responses of truss spar platforms.

References

Cao, P., Zhang, J., 1996. Slow motion responses of compliant offshore structures. In: Proceeding of the Sixth International Offshore and Polar Engineering Conference, vol. 1, pp. 296–303.

Technip Document No. KIK-TMM-30-NA-RP-1206-B, 2005. Inplace model test result correlation.

Johnson, R.P., 1995. Spar model test. Offshore Tech Res Center JIP Rept submitted to Deep Oil Technology, Inc.

Li, Y., Kareem, A., 1992. Computation of wave-induced drift forces introduced by displaced position of compliant offshore platforms. Journal of Offshore Mechanics and Arctic Engineering 114 (8), 175–184.

Longuet-Higgins, M.S., Steward, R.W., 1960. Changes in the form of short gravity waves and tidal currents. Journal of Fluid Mechanics 8, 575–583.

Mekha, B.B., Johnson, Roesset, J.M., 1995. Nonlinear response of spar in deep water: different hydrodynamic and structural models. In: Proceeding of the Fifth International Offshore and Polar Engineering Conference, vol. 3, pp. 462–469.

Mekha B.B., Weggel D., Johnson C.P., Roesset J.M., 1996. Effects of second order diffraction forces on the global response of spars. In: Proceeding of the Sixth International Offshore and Polar Engineering Conference, vol. 1, pp. 273–280.

Perryman, S.R., Beynet, P.A., 1994. Deepwater surface production and riser systems. In: Proceedings of Offshore and Arctic Operations Symposium, New Orleans, LA, January 23–24.

Rainey, R.C.T., 1989. A new equation for calculating wave loads on offshore structures. Journal of Fluid Mechanics 204, 295–324.

Ran, Z., Kim, M.H., 1997. Nonlinear coupled responses of a tethered spar platform in waves. International Journal of Offshore and Polar Engineering 7 (2), 27–34.

Ran, Z., Kim, M.H., Niedzwecki, J.M., Johnson, R.P., 1996. Responses of a spar platform in random waves and currents (Experimental vs. Theory). International Journal of Offshore and Polar Engineering 6 (1), 27–34.

Ran, Z., Kim, M.H., Zheng, W., 1998. Coupled dynamic analysis of a moored spar in random waves and currents (time-domain vs. frequency-domain analysis). Journal of Offshore Mechanics and Arctic Engineering 121, 194–200.

Rudnick, P., 1964. FLIP: an Oceanographic buoy. Science 146, 1268–1273.

Rudnick, P., 1967. Motion of a large spar buoy in sea waves. Journal of Ship Research 11, 257–267.

Zehang, J., Chen, L., Ye, M., Randall, R.E., 1995. Hybird wave model for unidirectional irrigular waves, part I: theory and numerical scheme. Applied Ocaean Research 18, 77–92.